

Minority-carrier kinetics in heavily doped GaAs:C studied by transient photoluminescence

A. Maaßdorf, S. Gramlich, E. Richter, F. Brunner, M. Weyers, and G. Tränkle
Ferdinand-Braun-Institut, Albert-Einstein-Strasse 11, 12489 Berlin, Germany

J. W. Tomm,^{a)} Y. I. Mazur, D. Nickel, V. Malyarchuk, T. Günther, Ch. Lienau, A. Bärwolff,
 and T. Elsaesser
Max-Born-Institut, Max-Born-Strasse 2 A, 12489 Berlin, Germany

(Received 16 April 2001; accepted for publication 11 January 2002)

Room-temperature photoluminescence decay time measurements in heavily doped GaAs:C-layers designed as base layers for heterojunction bipolar transistors are reported. These measurements provide access to nonequilibrium minority carrier lifetimes that determine the current gains of those devices. By systematically studying transient luminescence spectra over a wide range of excitation densities between 10^{13} and 10^{18} cm^{-3} , we demonstrate the importance of carrier trapping processes at low excitation densities. Optimized excitation conditions that achieve trap saturation but also avoid stimulated emission are found for densities of $(1-3) \times 10^{17}$ cm^{-3} /pulse. Detection is limited to a spectral window well above the energy gap (beyond 1.5 eV). Values for both Auger and radiative recombination coefficients are given. © 2002 American Institute of Physics.

[DOI: 10.1063/1.1456244]

I. INTRODUCTION

Heterojunction bipolar transistors (HBTs) with a heavily *p*-doped GaAs:C base [$p_0 = (1-5) \times 10^{19}$ cm^{-3}] are of substantial importance for high-frequency power amplification systems used in communication systems such as in cellular phones. The HBT current gain β , i.e., the amplification of the HBT device, is proportional to the minority-carrier lifetime τ within the base of those transistors

$$\beta = (2kT/e)\mu\tau/W_B^2 - 1. \quad (1)$$

Here k denotes the Boltzmann constant, T the temperature, e the elementary charge, μ the minority carrier mobility, and W_B the width of the base layer. Thus τ is a key parameter governing device performance. In addition, device lifetime and reliability are also strongly affected by τ .¹ Thus accurate measurement of τ and subsequent control of this parameter by proper adjustment of epitaxial growth parameters is essential for optimizing the device characteristics.

Moreover, such materials are of interest for studying the effects of extremely high doping concentrations [$p_0 = (1-5) \times 10^{19}$ cm^{-3}] on minority carrier recombination dynamics. Here, it is of importance that the intentional creation of such high carrier concentrations by doping gives rise to defect creation and to pronounced modifications of the band structure via both band gap renormalization and modifications of the density of states (DOS), in particular through pronounced defect-related tail states. Minority carrier recombination kinetics is therefore generally affected by a complex interplay between different physical processes. *Intrinsic* recombination mechanisms, such as radiative and Auger recombination as well as *extrinsic* mechanisms, such as defect-

related recombination and surface and/or interface recombination, contribute to the recombination dynamics. This generally gives rise to a significant excitation density dependence of the resulting effective minority-carrier recombination rates. This effective lifetime τ_{eff} is described as a sum of the recombination rates for all individual processes, i.e.,

$$\begin{aligned} \frac{1}{\tau_{\text{eff}}} &= \frac{1}{\tau_{\text{rad}}} + \frac{1}{\tau_{\text{aug}}} + \frac{1}{\tau_t} + \frac{2S}{d} \\ &= Bp + Cp^2 + \frac{1}{\tau_t(n)} + \frac{2S}{d}, \end{aligned} \quad (2)$$

where $1/\tau_{\text{rad}} = Bp$ and $1/\tau_{\text{aug}} = Cp^2$ describe the inverse radiative and Auger recombination lifetimes that are generally assumed to be independent of the minority carrier density, if $\delta n = \delta p \ll p_0$. The trapping rate $1/\tau_t(n)$ on the other hand may show a pronounced dependence on δn , reflecting trap saturation. The phenomenological parameter $2S/d$ describes carrier recombination at the interfaces, with S being the interface recombination velocity and d the layer thickness.

One possibility to experimentally access τ is to analyze transient photoluminescence (PL) data after short impulsive laser excitation. This approach relies on the assumption of a linear relationship between the PL signal and nonequilibrium carrier density ($\delta n = \delta p$), i.e., the PL signal is used to probe δn . Thus the PL decay time τ_d , i.e., the time constant of the transient PL decay, is identified with τ_{eff} introduced in Eq. (2). Here, in particular room temperature data are relevant for device characterization.

Different transient PL studies of heavily doped GaAs:C have been reported so far.²⁻⁹ A series of articles by Strauss *et al.*,⁴ Heberle *et al.*,⁵ and Strauss *et al.*⁶ focuses on this interplay between intrinsic and extrinsic parameters in free

^{a)} Author to whom correspondence should be addressed; electronic mail: tomm@mbi-berlin.de

GaAs:C layers. In particular, the effects of surface recombination on the recombination dynamics are addressed in detail in these studies. Benchimol *et al.*^{7,8} and Ahrenkiel *et al.*⁹ circumvent the effects of recombination at the free surfaces by investigating transient PL of AlGaAs/GaAs:C/AlGaAs structures. Values for radiative and Auger recombination coefficients were obtained. Yet these studies have mostly been performed within a limited range of excitation densities thus calling for detailed density-dependent investigation of the recombination dynamics. Such a study at room temperature is explicitly reported in this article.

The article is organized as follows. After a brief introduction and analysis of the stationary room-temperature PL spectra, we discuss transient PL data recorded on different highly doped GaAs:C layers over a wide range of excitation densities between $\delta n = 10^{13}$ and 10^{18} cm⁻³. The PL decay curves are analyzed within a phenomenological rate equation model incorporating radiative and Auger recombination and carrier trapping into defect states. Coefficients for radiative and Auger recombination in these materials are estimated. Finally, we draw some conclusions.

II. EXPERIMENT

A Ti:sapphire laser system with a pulse duration of less than 100 fs and a repetition rate of 82 MHz is used for impulsive interband excitation at a wavelength of 735 nm. The delay of 12.2 ns between successive pulses is sufficiently long to avoid substantial influence on the *initial* PL decay. Nonequilibrium carrier densities between $\delta n = 10^{13}$ and 10^{18} cm⁻³ are generated per pulse. Transient PL is detected by a streak camera in synchro-scan mode. Spectral selection is provided by dispersing the PL in a 0.25 m monochromator. The experiments are performed with a spot size of the laser focus of $\varnothing_{\text{FWHM}} = 200$ μm . The overall temporal resolution of the setup is better than 20 ps ($1/e$ decay). Steady-state PL spectra are measured with standard equipment.

The near-field scanning optical microscope (NSOM) used in an illumination/collection geometry for PL measurements at cleaved sample edges is described in Ref. 10.

In order to estimate the effects of doping on the DOS, Urbach parameters E_0 , i.e., the slopes of the exponential part of the absorption constant below the energy gap E_g , are determined by photocurrent and PL measurements. We find values of $E_0 = 16$ – 24 meV at 295 K and E_0 tend to increase with the doping level.

The investigated double heterostructures are grown by metalorganic chemical vapor deposition (MOCVD) in a horizontal Aixtron AIX200 reactor on GaAs substrates. Trimethylgallium [$\text{Ga}(\text{CH}_3)_3$] as a group-III precursor together with Arsin (AsH_3) enable intrinsic incorporation of carbon into the GaAs layers by choosing the V/III ratio near unity at a growth temperature below 600 °C. Two groups of clad samples, either with $\text{Ga}_x\text{In}_{1-x}\text{P}$ or $\text{Al}_x\text{Ga}_{1-x}\text{As}$ barriers, are investigated. The $\text{Al}_x\text{Ga}_{1-x}\text{As}$ barrier layers have a composition of $x = 0.28$ [cf. Fig. 1(a), structure I]. The $\text{Ga}_x\text{In}_{1-x}\text{P}$ barriers are grown at 580 °C with a mole fraction of x

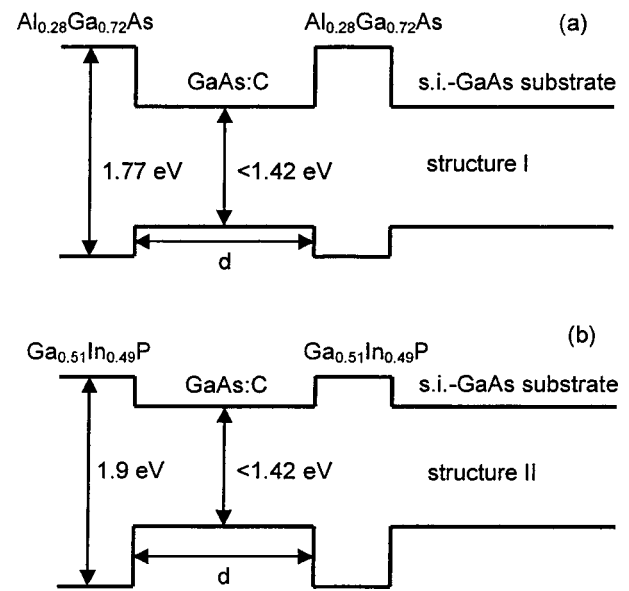


FIG. 1. Schematic of the two types of heterostructures investigated: carbon doped GaAs layers clad between (a) $\text{Al}_{0.28}\text{Ga}_{0.72}\text{As}$ barriers (structure I) and (b) $\text{Ga}_{0.51}\text{In}_{0.49}\text{P}$ barriers (structure II).

$= 0.51$ to achieve lattice matching with GaAs [cf. Fig. 1(b), structure II].

III. RESULTS AND DISCUSSION

A. Room-temperature PL spectra from GaAs:C

Figures 2(a) and 2(b) show stationary room-temperature PL spectra measured with time-integrating detection for cw and fs excitation, respectively. Data from four samples clad by InGaP barriers and with carrier concentrations of $p_0 = (1-5) \times 10^{19}$ cm⁻³ are compared. No systematic differences are found between spectra recorded with cw excitation [Fig. 2(a)] or fs excitation with an excitation density of $\delta n = 3 \times 10^{17}$ cm⁻³/pulse [cf. Fig. 2(b)]. Also the effective carrier temperatures estimated from the high-energy tail of the spectra are similar and close to room temperature [cf. inset in Fig. 2(b)]. This suggests that carrier heating due to fs excitation, as observed already before in stationary PL spectra of GaAs (Ref. 11) and, in particular, in heavily doped GaAs:C (Ref. 12) is of minor importance at least under our experimental conditions.

All PL spectra display a clear double peak structure that exhibits a systematic line shape variation with increasing p_0 . Such a double peak spectrum was observed before.¹³⁻¹⁵ Different explanations were given. The systematic dependence on doping concentration led the authors of Ref. 13 to conclude that the lower energy peak is a defect-related transition. On the other hand, it was suggested that the double structure arises from two different contributions to the PL:^{14,15} (i) The “regular” PL emitted into the direction of the collection optics and (ii) PL that is emitted into the substrate direction, propagates through the substrate, and is back reflected at the GaAs/Air interface at the bottom of the substrate. These two contributions are schematically illustrated in Fig. 3(a). For the back-reflected PL contribution, the substrate acts as a spectral edge filter strongly suppressing lumi-

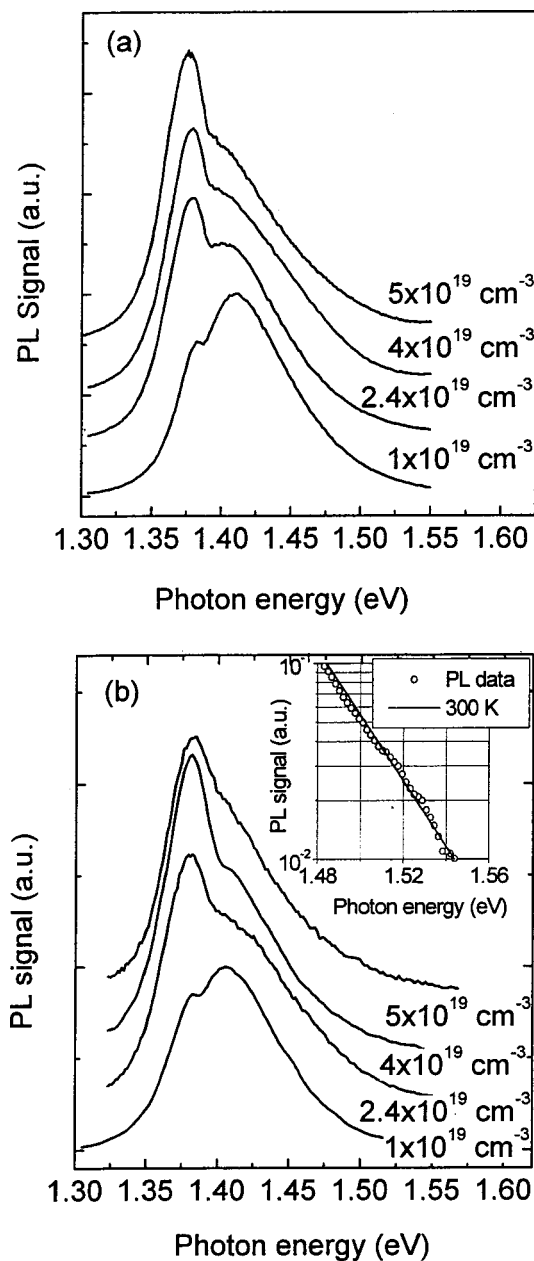


FIG. 2. (a) Room-temperature cw PL spectra for four samples clad by GaInP barriers (structure II) with carbon doping concentrations of 1, 2.4, 4, and $5 \times 10^{19} \text{ cm}^{-3}$ and a thickness of the GaAs:C layer of $1 \mu\text{m}$. The excitation wavelength is 735 nm. (b) Room-temperature PL spectra for the same samples excited with 735 nm fs pulses creating a density of about $3 \times 10^{17} \text{ cm}^{-3}$ pulse. The inset shows the data from the spectrum for the sample with $p_0 = 1 \times 10^{19} \text{ cm}^{-3}$ on a semilogarithmic scale and the kT slope for $T = 300 \text{ K}$.

nescence above the substrate's band gap energy. Within this model the observed systematic increase of the lower energy PL contribution to the double peak structure with doping is caused by the redshift of the PL emission due to band gap renormalization within the heavily doped layer that is of major importance in highly doped materials.¹⁴

A clear distinction between the two alternative explanations can be made by comparing macroscopic spectra to those recorded with a NSOM. Figure 3(c) compares a conventional cw PL spectrum obtained in far-field PL geometry [cf. Fig. 3(a)] and a cw spectrum that was excited and col-

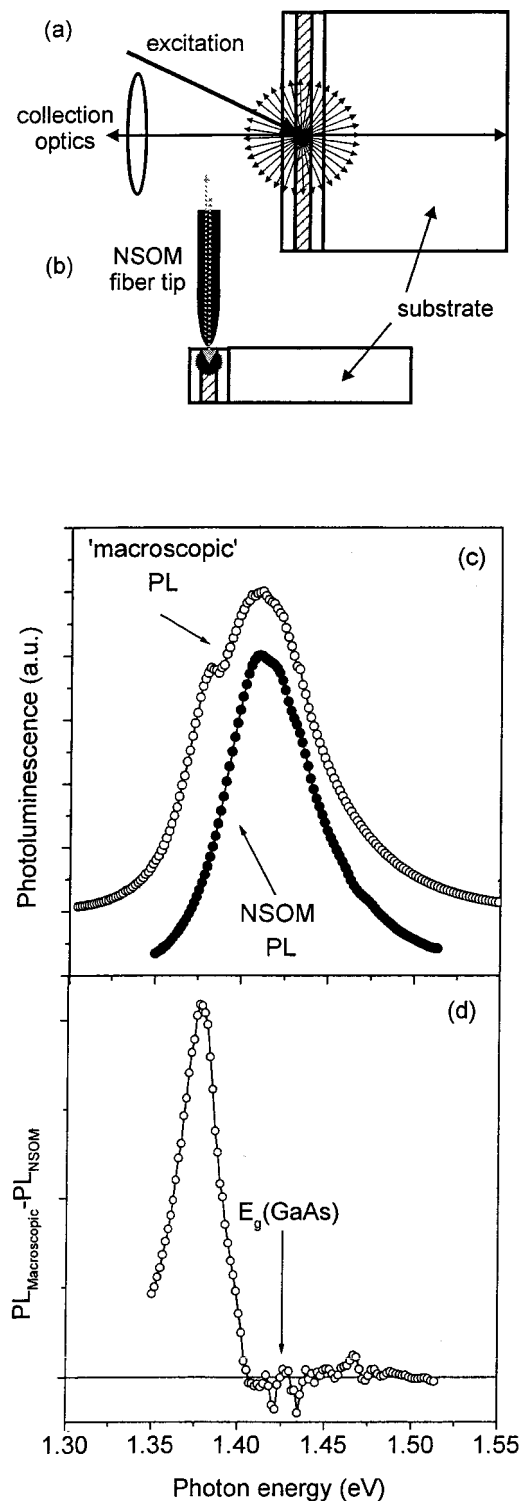


FIG. 3. (a) Schematic of the macroscopic cw PL excitation and detection scheme. The PL data are obtained by excitation through the top cladding by creating an excitation spot of $\varnothing = 200 \mu\text{m}$. (b) Schematic of the NSOM based cw PL excitation and detection scheme. The near-field microscope is operated in illumination/collection geometry, i.e., the sample is locally excited through the NSOM fiber and PL is collected through the same fiber. (c) Macroscopic and NSOM based cw PL data from the same sample ($p_0 = 1 \times 10^{19} \text{ cm}^{-3}$). The macroscopic PL spectrum shows a clear double peak structure, whereas a single PL emission peak is observed in the NSOM configuration. (d) The difference spectrum between normalized macroscopic and near-field spectra shows a clear cutoff slightly below the band edge of the substrate material. This assigns the second, low energy peak in the macroscopic PL to emission that propagates through the substrate and is back reflected from the GaAs/Air interface at the bottom of the substrate.

lected through the fiber tip of the NSOM as schematically shown in Fig. 3(b). In this microscopic geometry back-reflected PL contributions propagating through the substrate and being picked up by the NSOM tip again are negligible and we expect to collect only PL being directly emitted in the direction of the NSOM fiber probe. Indeed, we observe a single-peaked PL spectrum with a substantially reduced full width at half maximum of about 62 meV. The difference between normalized macroscopic and near-field spectra [Fig. 3(d)] shows a clear cutoff slightly below the band edge position of the substrate. This directly demonstrates that the second lower energy peak in the far-field spectrum can be unequivocally assigned to PL that is emitted into the substrate direction, propagates through the substrate, and is back reflected at the bottom of the sample. The line broadening of the regular PL peak seen in the near-field spectrum is close to the value of $1.8 \times kT = 46$ meV expected for room-temperature k -conserving spontaneous emission without degeneracy and $E_0 = 0$. The remaining broadening is easily explained by the presence of defect related tail states described by an Urbach parameter of $E_0 = 16\text{--}24$ meV, cf. Sec. II.

B. Transient PL data from GaAs:C

In this section, we discuss transient PL decay curves recorded over a wide range of excitation densities: $\delta n = (10^{13}\text{--}10^{18})\text{ cm}^{-3}$. Figure 4 shows transients that are recorded on two different samples in a spectral detection window at about 1.5 eV, i.e., well above $E_g(\text{GaAs}) = 1.424$ eV, and even more above the E_g of the heavily doped gap-shrunk material. The behavior of both samples is clearly different. The first sample [cf. Fig. 4(a)] a GaAs layer ($p_0 = 2 \times 10^{19}\text{ cm}^{-3}$) is clad by $\text{Al}_{0.28}\text{Ga}_{0.72}\text{As}$ barriers (structure I). The transient PL is characterized by a single-exponential decay with a decay time that is slightly increasing with increasing δn . The second sample [cf. Fig. 4(b)], consists of a GaAs layer ($p_0 = 10^{19}\text{ cm}^{-3}$) clad by $\text{Ga}_{0.51}\text{In}_{0.49}\text{P}$ barriers (structure II). The PL decay curves of this sample show a pronounced biexponential decay behavior at low excitation densities that is gradually transformed into a single-exponential decay as δn is increased.

In order to clarify the nature of the fast transient in Fig. 4(b), transient spectra are recorded within the 100–200 and 500–600 ps time windows, i.e., in regions where, respectively, the fast and slow process dominate the recombination behavior. Both spectra have exactly the same shape. This indicates, together with the conclusions from Sec. III A, that the fast and saturable decay process in Fig. 4(b) can be assigned to a *nonradiative* recombination process, most likely carrier trapping into defect states. The assignment is supported by the finding that a pronounced biexponential behavior appears predominantly for one special sample group, namely for InGaP/GaAs:C/InGaP structures. The observed effect, however, is also present for other samples including bulk GaAs reference samples, even though less pronounced than in Fig. 4(b). Intrinsic recombination processes, such as radiative and Auger recombination, are characterized rather by a decrease of τ with increasing δn and can clearly not account for this saturable biexponential decay.

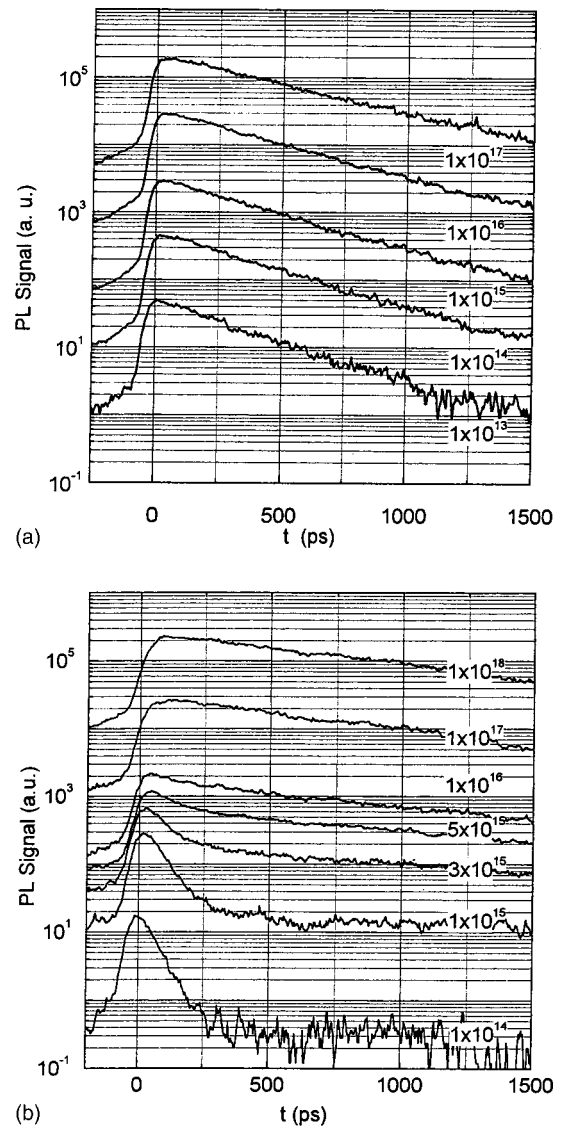


FIG. 4. (a) Room-temperature transient PL data from sample A ($d = 1\text{ }\mu\text{m}$, AlGaAs barriers, $p_0 = 2 \times 10^{19}\text{ cm}^{-3}$). The parameter is the excitation density per pulse that is varied between 10^{13} and 10^{17} cm^{-3} . (b) Room-temperature transient PL data from sample B ($d = 1\text{ }\mu\text{m}$, InGaP barriers, $p_0 = 1 \times 10^{19}\text{ cm}^{-3}$). The parameter is the excitation density per pulse that is varied between 10^{14} and 10^{18} cm^{-3} .

To qualitatively describe the measured recombination dynamics, we use a phenomenological rate equation model based on a simplified three-level scheme, as depicted in Fig. 5(a). The different levels represent the conduction band edge E_c , and the valence band edge E_v and a donor level E_D . The optical generation of nonequilibrium carrier pairs ($\delta n = \delta p$) is described by a generation term $G = G_0 \times \delta(t)$ and results in concentrations $n = n_0 + \delta n$ and $p = p_0 + \delta p$. The population (ionization) of the donor level E_D with a density of N^D is represented by N^{D+} . The population of the three levels is described by the following coupled rate equation system:

$$\begin{aligned} \frac{\partial n}{\partial t} &= G - Bpn - Cp^2n + e_n \cdot (N^D - N^{D+}) \\ &- \alpha_n N^{D+} n, \end{aligned} \quad (3)$$

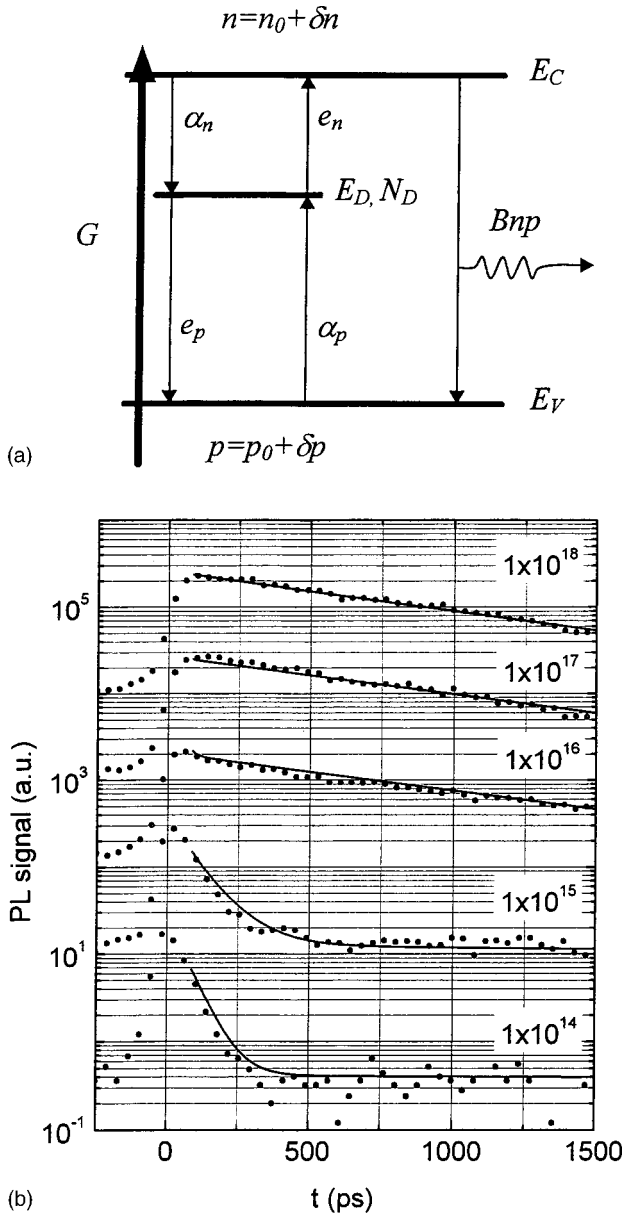


FIG. 5. (a) Scheme of a simplified three-level system, consisting of conduction band E_C , valence band E_V , and donor level E_D with a concentration N_D . α_n , α_p and e_n , e_p are capture probabilities and emission rates for electrons and holes, respectively. The optical generation of nonequilibrium carrier pairs ($\delta n = \delta p$) is described by a generation term G and results in concentrations $n = n_0 + \delta n$ and $p = p_0 + \delta p$, whereas Bnp represents the radiative recombination rate. (b) Selected room-temperature transient PL data from sample B [Fig. 4(b)]. The number of presented data points per curve is reduced to highlight the comparison between data and simulation. Solid lines represent the fit to the rate equation model. The generation rate G used in the fitting procedure was scaled linearly with the experimental excitation density.

$$\frac{\partial N^{D+}}{\partial t} = -(\alpha_n n + e_p) \cdot N^{D+} + (\alpha_p p + e_n) \cdot (N^D - N^{D+}), \quad (4)$$

$$\frac{\partial p}{\partial t} = G - Bnp - Cp^2 n + e_p N^{D+} - p \alpha_p \cdot (N^D - N^{D+}). \quad (5)$$

α_n , α_p and e_n , e_p are capture probabilities and emission rates for electrons and holes, respectively. With $\alpha_n = 1/(N^D \times \tau_i)$ and a trapping time of $\tau_i = 65$ ps [taken from the fast transient in Fig. 4(b)] the rate equation system is solved by Runge–Kutta integration. Accumulation effects due to the high repetition rate (82 MHz) are taken into account in the simulations [iterative solution of Eqs. (3)–(5)]. Selected transients from Fig. 4(a) are numerically fit to the simulated $\delta n(t)$ curves [cf. Fig. 5(b)]. The parameters of the model are estimated in this way to be $N^D = 3 \times 10^{15} \text{ cm}^{-3}$, $\alpha_n = 5.1 \times 10^{-6} \text{ cm}^{-3} \text{ s}^{-1}$, $\alpha_p = 6.7 \times 10^{-13} \text{ cm}^{-3} \text{ s}^{-1}$, $e_n = 3.1 \times 10^8 \text{ s}^{-1}$, and $e_p = 1.55 \times 10^{-13} \text{ s}^{-1}$. Obviously the interaction of the traps with holes described by α_p and e_p is negligible. We should note that the whole rate equation model is symmetric with respect to exchanging the donor by an acceptor like trap state. The consistent fit of the PL decay with finally only two completely independent parameters as well as the determination of a realistic value of $N^D = 3 \times 10^{15} \text{ cm}^{-3}$ are additional arguments for the presence of deep level defects in some of our samples. Thus the simplified three-level model allows one to account for the different effects observed in our PL studies, namely the biexponential PL decay dynamics and the pronounced long-lived component of the PL decay curves over an excitation range of 5 orders of magnitude.

These results indicate clearly that the room-temperature intrinsic minority carrier recombination dynamics, unaffected by carrier trapping, can only be investigated at relatively high excitation densities sufficient to saturate the trap states.

Next, we discuss the spectral dependence of the PL decay times in this high excitation density regime. One such set of data taken for $\delta n = \delta p = 3 \times 10^{17} \text{ cm}^{-3}/\text{pulse}$ is shown in Fig. 6 together with the PL spectrum. The positions of the energy gaps are also indicated in the figure. As the detection energy is scanned across the luminescence band, the PL decay decreases monotonically from 1.85 ns at photon energies below 1.35 eV to 1.4 ns at energies above 1.5 eV. Such photon energy dependent transient PL behavior is well known, in particular from low-temperature PL studies of excitons localized in alloy potential fluctuations¹⁶ or carrier pairs confined in quantum dots¹⁷ that show a certain size distribution. It generally reflects carrier localization in minima of a disordered potential. In our case, this disorder potential reflects the defect induced tail states around the band edge. The recombination time of these localized states is increased as compared to the intrinsic recombination time out of high-energy states. Hence, in order to obtain at least reproducible PL decay times, the detection energy should be set to the high energy region above the band edge, >1.5 eV, showing detection-energy independent PL decay times.

C. Nonequilibrium carrier lifetimes

So far, we did not address the role of carrier recombination at the interfaces of the doped layers. In this last section, we analyze the influence of interface recombination by investigating a set of samples with different layer thicknesses. This widely used method was introduced by Ahrenkiel

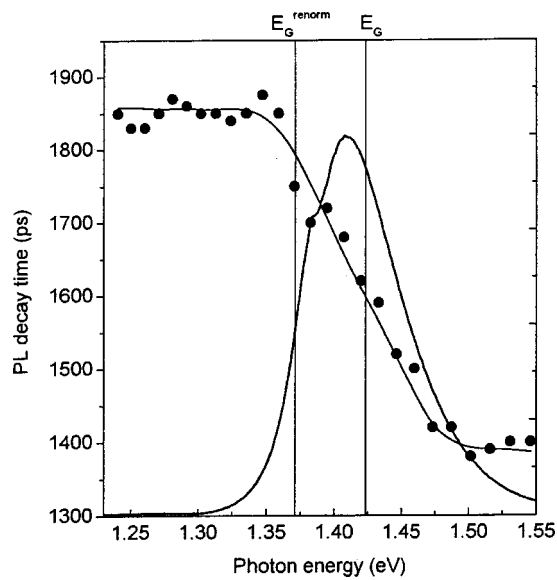


FIG. 6. PL decay time vs photon energy for a sample (structure I) with a $N_A = 10^{19} \text{ cm}^{-3}$. For comparison a PL spectrum is added. The decay time shows a monotonic decrease as the detection energy is scanned toward higher photon energies across the band edge. This is ascribed to carrier localization in defect related tail states at the band edge.

*et al.*¹⁸ (see also Ref. 19 and for a description of relevant methodology, Ref. 20). Figure 7 shows a plot of the reciprocal PL decay time versus inverse sample thickness. The data show a clear reduction of the PL decay time with decreasing layer thickness, indicating that interface recombination is indeed important in this set of samples. Within the model introduced in Ref. 18 the layer thickness dependence of the PL decay times is given by

$$1/\tau_d = 1/\tau + 2S/d, \tag{6}$$

where τ indicates the lifetime of the bulk material, τ_d the PL decay time, S the interface recombination velocity, and d the

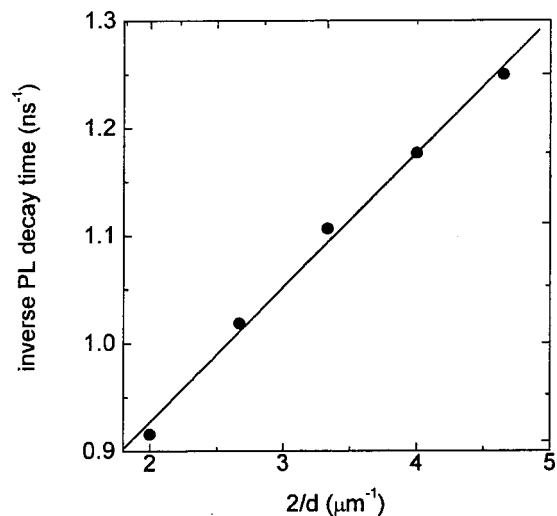


FIG. 7. Inverse PL decay time vs reciprocal sample thickness for a set of five samples with $N_A = 10^{19} \text{ cm}^{-3}$. The linear increase in the PL decay rate with inverse sample thickness is ascribed to minority carrier recombination at the GaAs/barrier interfaces [Eq. (6)]. From the linear fit we determine $\tau = 1.6 \text{ ns}$ and $S = 1.4 \times 10^4 \text{ cm s}^{-1}$.

layer thickness. Assuming a constant value of τ for all samples we find good agreement between experiment and model for $\tau = 1.6 \text{ ns}$ and $S = 1.4 \times 10^4 \text{ cm s}^{-1}$. A detailed description of these experiments is published elsewhere.³

The data discussed in Sec. III indicate that reliable information on intrinsic nonequilibrium carrier recombination in heavily doped GaAs, namely via radiative and Auger recombination, can be extracted from our transient PL data under carefully chosen excitation conditions. First, the excitation density should be chosen in the range of $(1-3) \times 10^{17} \text{ cm}^{-3}$ in order to achieve trap saturation. Second, the detection photon energy should be well above the band edge, to avoid localization effects on the PL decay. And third, it is important to investigate sets of samples with different layer thicknesses, in order to sort out interface recombination effects [see Eq. (6)].

We now extract this information on intrinsic recombination mechanisms from a series of density-dependent decay time measurements on various sample sets with doping concentrations between 1 and $5 \times 10^{19} \text{ cm}^{-3}$. The results are summarized in Fig. 8 together with the calculated density dependence of the intrinsic radiative recombination (dashed line) and Auger recombination mechanism (dotted line).⁶ The solid line in Fig. 8 represents the total $1/\tau = 1/\tau_r + 1/\tau_A$. Some of the data points, each from a sample set (with various thickness), exactly match the calculated theoretical density dependence limits. We consider this an excellent confirmation of the success of our attempts to at least minimize the impact of extrinsic effects to our data, and can extract the coefficients for radiative and Auger recombination as $B = 0.5 \times 10^{-10} \text{ cm}^3 \text{ s}^{-1}$ and $C = 4 \times 10^{-30} \text{ cm}^6 \text{ s}^{-1}$. The latter number remarkably agrees with $C = 6 \times 10^{-30} \text{ cm}^6 \text{ s}^{-1}$ published recently by Ahrenkiel *et al.*⁹ for GaAs:C with $p_0 = 1 \times 10^{19} \text{ cm}^{-3}$.

We also added some data obtained by Benchimol *et al.*^{7,8} and Ahrenkiel *et al.*⁹ to Fig. 8. Small τ values are likely to indicate the presence of additional recombination channels, e.g., of Shockley–Read–Hall type, or insufficient trap saturation.

IV. CONCLUSIONS

Transient PL from heavily doped GaAs:C is studied with the main objective to derive reliable room-temperature non-equilibrium carrier lifetime data. Analysis of steady state and transient PL spectra indicate the absence of pronounced hot electron effects at room temperature for excitation densities of $10^{17} - 10^{18} \text{ cm}^{-3}$ /pulse. We show that a doublet structure present in all room-temperature PL spectra is caused by a geometrical effect.

We find that reproducible PL decay time measurements require:

- (i) relatively high excitation densities of $\delta n = \delta p > 1 \times 10^{17} \text{ cm}^{-3}$ /pulse as well as
- (ii) detection within a spectral window well above the gap ($> 1.5 \text{ eV}$ at 295 K).

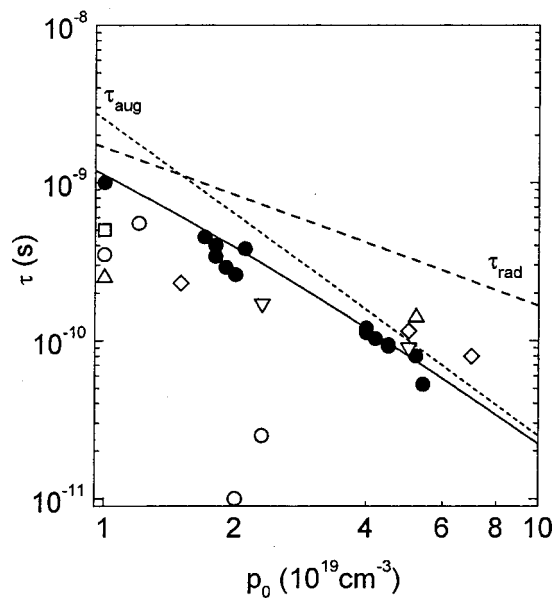


FIG. 8. Nonequilibrium carrier lifetimes τ (full circles) vs carrier concentration for 15 sample sets derived from time-resolved PL decay measurements. The data were recorded at excitation densities of $3 \times 10^{17} \text{ cm}^{-3}$, ensuring trap saturation. In all cases, the detection energies were chosen well above E_g ($> 1.5 \text{ eV}$), minimizing localization effects (see Fig. 6). Each data point is obtained by analyzing a set of samples of different layer thicknesses and the intrinsic lifetime was extrapolated according to Eq. (5), (see Fig. 7). Radiative (dashed line) and Auger lifetime (dotted line) are calculated according to Ref. 6. The full lines represent total lifetimes $1/\tau = 1/\tau_{\text{aug}} + 1/\tau_{\text{rad}}$. The data obtained in this work (full circles) are compared to data obtained by Benchimol *et al.* (see Refs. 7 and 8) (open triangles and rhombs) and Ahrenkiel *et al.* (see Ref. 9) (open squares and circles) and references therein.

The latter implies that in some cases only a small fraction of the total PL can be used for reliable PL decay time measurements.

Data from several sample sets (thickness variation) are well explained by assuming the exclusive presence of Auger and radiative recombination. There is a tendency for comparable doping level AlGaAs/GaAs:C/AlGaAs samples to show longer lifetime values compared to GaInP/GaAs:C/GaInP samples (cf. Ref. 3). The coefficients for radiative and Auger recombination are determined to be $B = 0.5 \times 10^{-10} \text{ cm}^3 \text{ s}^{-1}$ and $C = 4 \times 10^{-30} \text{ cm}^6 \text{ s}^{-1}$.

The identification of the microscopic nature of the contributions by deep levels and tail states will be a task for further work. It would be very useful to find out whether

they are homogeneously distributed in the GaAs:C or GaAs bulk or rather located at the interfaces. Recent experiments with intentionally treated GaAs bulk surfaces indicate that at least the trapping time depends sensitively on the surface condition.

Thus we have shown how PL decay time measurements can be used for MOCVD growth optimization as well as for the estimation of expected HBT current gains on the wafer scale immediately after epitaxial growth.

ACKNOWLEDGMENTS

The authors would like to thank V. Petrov for experimental help. They also thank J. Koch for PL measurements.

- ¹Q. Yang, D. S. Scott, T. Chung, and G. E. Stillman, *Appl. Phys. Lett.* **77**, 271 (2000).
- ²H. Ito, T. Furuta, and T. Ishibashi, *Appl. Phys. Lett.* **58**, 2936 (1991).
- ³F. Brunner *et al.*, *J. Electron. Mater.* **29**, 205 (2000).
- ⁴U. Strauss, A. P. Heberle, X. Q. Zhou, W. W. Rühle, T. Lauterbach, K. H. Bachem, and N. M. Haegel, *Jpn. J. Appl. Phys., Part 1* **32**, 495 (1993).
- ⁵A. P. Heberle, U. Strauss, W. W. Rühle, K. H. Bachem, T. Lauterbach, and N. M. Haegel, *Extended Abstracts International Conference on Solid State Devices and Materials*, Tsukuba, Japan, 1992, p. 290.
- ⁶U. Strauss, W. W. Rühle, and K. Köhler, *Appl. Phys. Lett.* **62**, 55 (1993).
- ⁷J. L. Benchimol, F. Alexandre, C. Dubon-Chevallier, F. Heliot, R. Bourguiga, J. Dangla, and B. Sermage, *Electron. Lett.* **28**, 1344 (1992).
- ⁸J. L. Benchimol, F. Alexandre, N. Jourdan, A. M. Pougnet, R. Mellet, B. Sermage, F. Heliot, and C. Dubon-Chevallier, *J. Cryst. Growth* **127**, 690 (1993).
- ⁹R. K. Ahrenkiel, R. Ellingson, W. Metzger, D. I. Lubyshev, and W. K. Liu, *Appl. Phys. Lett.* **78**, 1879 (2001).
- ¹⁰Ch. Lienau, A. Richter, and J. W. Tomm, *Appl. Phys. A: Mater. Sci. Process.* **64**, 341 (1997).
- ¹¹M. van Driel, X.-Q. Zhou, W. W. Rühle, J. Kuhl, and K. Ploog, *Appl. Phys. Lett.* **60**, 2246 (1992).
- ¹²B. J. Aitchison, N. M. Haegel, C. R. Abernathy, and S. J. Pearton, *Appl. Phys. Lett.* **56**, 1154 (1990).
- ¹³H. D. Chen, M. S. Feng, P. A. Chen, K. C. Lin, and J. W. Wu, *Jpn. J. Appl. Phys., Part 1* **33**, 1920 (1994).
- ¹⁴J.-S. Lee, I. Kim, B.-D. Choe, W. G. Jeong, Y. K. Sin, and W. S. Min, *J. Appl. Phys.* **79**, 9278 (1996).
- ¹⁵Z. H. Lu and A. Majerfeld, *J. Appl. Phys.* **75**, 2648 (1994).
- ¹⁶C. Gourdon and P. Lavallard, *Phys. Status Solidi B* **153**, 641 (1989).
- ¹⁷Yu. I. Mazur, J. W. Tomm, V. Petrov, G. G. Tarasov, H. Kissel, C. Walther, Z. Ya. Zhuchenko, and W. T. Masselink, *Appl. Phys. Lett.* **78**, 3214 (2001).
- ¹⁸R. K. Ahrenkiel, D. J. Dunlavy, and T. Hanak, *Sol. Cells* **24**, 339 (1988).
- ¹⁹R. K. Ahrenkiel, *Minority-Carrier Lifetime in III-V Semiconductors: Physics and Applications, in Semiconductors, and Semimetals*, edited by R. K. Willardson, A. C. Beer, and E. R. Weber (Academic, New York, 1993), Vol. 39.
- ²⁰G. B. Lush, M. R. Melloch, M. S. Lundstrom, D. H. Levi, R. K. Ahrenkiel, and H. F. MacMillan, *Appl. Phys. Lett.* **61**, 2440 (1992).